Limnol. Oceanogr., 43(7), 1998, 1500–1510

Interpretation of measured concentration profiles in sediment pore water

Peter Berg[1]
Department of Environmental Sciences, University of Virginia, Charlottesville, Virginia 22903

Nils Risgaard-Petersen
Institute of Biological Science, Department of Microbial Ecology, University of Aarhus, Ny Munkegade, Bldg. 540, DK-8000 Aarhus C, Denmark; and National Environmental Research Institute, Department of Lake and Estuarine Ecology, Vejlsøvej 25, DK-8600 Silkeborg, Denmark

Søren Rysgaard
National Environmental Research Institute, Department of Lake and Estuarine Ecology, Vejlosovej 25, DK-8600 Sikeborg, Denmark

Abstract

A robust numerical procedure for biogeochemical interpretation and analysis of measured concentration profiles of solutes in sediment pore water has been developed. Assuming that the concentration-depth profile represents a steady state, the rate of net production or consumption as a function of depth can be calculated, together with the flux across the sediment–water interface. Three kinds of vertical transport can be included in the analysis: molecular diffusion, bioturbation, and irrigation. The procedure involves finding a series of least square fits to the measured concentration profile, followed by comparisons of these fits through statistical *F*-testing. This approach leads to an objective selection of the simplest production–consumption profile that reproduces the concentration profile. Because the numerical procedure is optimized with respect to speed, one prediction can typically be done in a few minutes or less on a personal computer. The technique has been tested successfully against analytical solutions describing the transport and consumption of O_2 in sediment pore water. In other tests, measured concentration profiles of O_2, NO_3^-, NH_4^+, and ΣCO_2 have been interpreted using the new procedure.

Concentration profiles in sediment pore water are used widely in studies of biogeochemical processes. Profiles on a macroscale are measured using a variety of methods, including in situ samplers (Sayles et al. 1976; Kuivila et al. 1989), dialysis cells, so-called peepers (Hesslein 1976; Brandl and Hanselmann 1991), slicing techniques (Reeburgh 1967; Emerson 1976; Thamdrup et al. 1994*a*), and gel samplers (Krom et al. 1994). High-resolution techniques that employ microelectrodes (Revsbech et al. 1980) are used to measure profiles on a submillimeter scale. Although a fair amount of information and understanding can be achieved by simple visual examination of these measured profiles, their full value is realized by applying modeling techniques to their interpretation. Such applications make it possible to achieve a much more precise prediction of the location of zones of production or consumption, the extent of these zones, and the resulting fluxes across the sediment–water interface.

In many studies, the movement of solutes in sediments has been attributed to a vertical diffusion phenomenon (Blackburn et al. 1994; Glud et al. 1994; Thamdrup et al. 1994*b*; Rysgaard and Berg, 1996). Vertical diffusion can be separated into two contributions: molecular diffusion and bioturbation (i.e., the diffusion-like transport caused by random movements of meiofauna). Other studies have shown clearly that irrigation (i.e., the pumping activity of tube-dwelling animals) can significantly influence the transport of solutes in sediments (Aller 1983; Pelegri et al. 1994; Wang and Van Cappellen, 1996). Although irrigation is obviously a three-dimensional problem (Aller 1980), it is possible to include irrigation in one-dimensional formulations using the nonlocal source-sink function suggested by Boudreau (1984). Assuming steady state conditions and neglecting the effect of pore water movements due to burial, compaction, groundwater flow, and wave action, the one-dimensional mass conservation equation that accounts for the effects of molecular diffusion, bioturbation, and irrigation is

$$\frac{d}{dx}\left(\varphi(D_s + D_B)\frac{dC}{dx}\right) + \varphi\alpha(C_0 - C) + R = 0, \quad (1)$$

where C is the pore water concentration, C_0 is the bottom water concentration, x is the depth, φ is the porosity, D_s is the molecular diffusivity corrected for tortuosity, D_B is the biodiffusivity, α is the irrigation coefficient, and R is the net rate of production (or consumption if R is negative) per unit

[1] Corresponding author.

Acknowledgments

We thank K. Jensen for construction of NO_3^- and NH_4^+ sensors and L. B. Petersen for construction of O_2 microsensors, L. P. Nielsen for valuable discussions, K. McGlathery and D. Canfield for reading the manuscript, and P. Van Cappellen, an anonymous reviewer, and B. P. Boudreau for their constructive reviews. This study was supported by grants from the Danish National Science Research Councils contract 9501025 (S. Rysgaard). This work is a contribution to the European Union ELOISE program (ELOISE no. 040) in the framework of the NICE project carried out under contract MAS3-CT-96-0048 (N. Risgaard-Petersen).

volume of sediment. (For further details see Boudreau, 1997.)

A few previous studies also have focused on the interpretation of measured concentration profiles in sediment pore water. Neglecting bioturbation and irrigation and assuming that D_s, φ, and R are constant with depth, the analytical solution of Eq. 1 is given by a parabola. By matching pieces of parabolas drawn on transparencies with sections of oxygen profiles, Nielsen et al. (1990) identified depth intervals of constant oxygen consumption. Revsbech et al. (1986) used a numerical solution of the non-steady-state version of Eq. 1 to predict oxygen consumption rates by assuming a consumption profile, running the model until steady state conditions were present, adjusting the consumption profile based on a visual comparison of the simulated and measured concentration profiles, and repeating the entire process until acceptable agreement was achieved. This trial and error procedure allows variations in D_s and φ with depth and has been used in several studies (Christensen et al. 1989; Dalsgaard and Revsbech 1992; Jensen et al. 1994). However, the repeated manual adjustment of the consumption profile based on visual comparisons can be time consuming, and more importantly, it lacks objectivity. A much higher level of objectivity and a fast working procedure are two of the advantages of the technique presented here, where a series of least squares fits to the measured concentration profile is obtained through multiple solutions of Eq. 1, followed by a selection of one particular fit through statistical F-testing.

Measured concentrations can be used to approximate dC/dx in Eq. 1 and, with known values of φ, D_s, D_B, and α, to calculate the value of R for every measured interior point in the sediment. This procedure will, in almost all cases, lead to strongly oscillating values of R with depth (referred to as the production profile below) that would be difficult to interpret. Our objective is to find the simplest production profile (least number of descriptive variables) that provides a good explanation for our measured data. In an earlier implementation of our procedure, we used analytical fitting functions such as orthogonal polynomials to fit the measured concentration profiles, but these often gave a poor representation of the flux at the top and the bottom of the concentration profile. This problem is effectively solved by replacing the analytical fitting functions with a numerical solution to Eq. 1.

Methods

The numerical solution to Eq. 1 is based on a control volume approach (Patankar 1980), which is used widely in the field of modeling fluid flow and heat transfer. The sediment column, and the diffusive boundary layer in the water column if included, is divided into N thin horizontal layers, or control volumes. A grid point is located in the center of each control volume, where values of φ, D_s, D_B, and α are known. The general discretization equation is now derived by integrating Eq. 1 over control volume number j (from $x_{j-1/2}$ to $x_{j+1/2}$), which has an extent of Δx_j. Assuming that the grid point values of φ, α, and R (referred to as φ_j, α_j, and R_j) prevail throughout the control volume, the integral becomes

$$\left(\varphi(D_s + D_B)\frac{dC}{dx}\right)_{j+1/2} - \left(\varphi(D_s + D_B)\frac{dC}{dx}\right)_{j-1/2} + (\varphi_j\alpha_j(C_0 - C_j) + R_j)\Delta x_j = 0. \quad (2)$$

The second term in Eq. 2 represents the diffusive flux over the surface $j - 1/2$. Assuming that the grid point values φ_{j-1}, D_{sj-1}, and D_{Bj-1} prevail throughout the control volume $j - 1$ and that the concentration over the distance from $j - 1$ to $j - 1/2$ is given by a straight line (which becomes exact when α_{j-1} and R_{j-1} go to zero), the second term in Eq. 2 can be expressed as in Eq. 3a. Making similar assumptions for the control volume j leads to Eq. 3b:

$$-\left(\varphi(D_s + D_B)\frac{dC}{dx}\right)_{j-1/2} = -\varphi_{j-1}(D_{sj-1} + D_{Bj-1}) \times \frac{C_{j-1/2} - C_{j-1}}{\frac{1}{2}\Delta x_{j-1}} \quad (3a)$$

$$-\left(\varphi(D_s + D_B)\frac{dC}{dx}\right)_{j-1/2} = -\varphi_j(D_{sj} + D_{Bj}) \times \frac{C_j - C_{j-1/2}}{\frac{1}{2}\Delta x_j}. \quad (3b)$$

Eliminating $C_{j-1/2}$ from Eqs. 3a and 3b gives

$$-\left(\varphi(D_s + D_B)\frac{dC}{dx}\right)_{j-1/2} = -\frac{2\varphi_{j-1}(D_{sj-1} + D_{Bj-1})\varphi_j(D_{sj} + D_{Bj})}{\Delta x_{j-1}\varphi_j(D_{sj} + D_{Bj}) + \Delta x_j\varphi_{j-1}(D_{sj-1} + D_{Bj-1})} \times (C_j - C_{j-1}). \quad (4)$$

The fraction expresses the averaging of $\varphi(D_s + D_B)$ over the distance from $j - 1$ to j and is known as the harmonic mean in the fields of soil science (Haverkamp and Vauclin 1979) and fluid dynamics (Patankar 1980). A common averaging procedure is to use the arithmetic mean value of $\varphi_{j-1}(D_{sj-1} + D_{Bj-1})$ and $\varphi_j(D_{sj} + D_{Bj})$, which is an appropriate choice where variations of φ, D_s, and D_B are given by a smooth curve. In situations where the diffusive boundary layer is included with a well-defined interface between the sediment and the water column, jumps in these parameters occur and the arithmetic averaging can lead to rather incorrect implications (Patankar 1980). In this situation, a more appropriate choice is the harmonic mean, which also works well when the variations of φ, D_s, and D_B are given by a smooth curve (Patankar 1980).

Using the approximation (Eq. 4) for the flux over the surface $j - 1/2$ in Eq. 2 and the equivalent expression for the flux over the surface $j + 1/2$, the general discretization equation yields

$$AA_jC_{j-1} + BB_jC_j + CC_jC_{j+1} = DD_j, \quad (5)$$

where the coefficients AA_j, BB_j, CC_j, and DD_j are defined by

$$AA_j = \frac{1}{\Delta x_j}\left(\frac{2\varphi_{j-1}(D_{sj-1}+D_{Bj-1})\varphi_j(D_{sj}+D_{Bj})}{\Delta x_{j-1}\varphi_j(D_{sj}+D_{Bj})+\Delta x_j\varphi_{j-1}(D_{sj-1}+D_{Bj-1})}\right)$$

$$BB_j = \frac{1}{\Delta x_j}\left(-\frac{2\varphi_{j-1}(D_{sj-1}+D_{Bj-1})\varphi_j(D_{sj}+D_{Bj})}{\Delta x_{j-1}\varphi_j(D_{sj}+D_{Bj})+\Delta x_j\varphi_{j-1}(D_{sj-1}+D_{Bj-1})} - \frac{2\varphi_j(D_{sj}+D_{Bj})\varphi_{j+1}(D_{sj+1}+D_{Bj+1})}{\Delta x_j\varphi_{j+1}(D_{sj+1}+D_{Bj+1})+\Delta x_{j+1}\varphi_j(D_{sj}+D_{Bj})}\right) - \varphi_j\alpha_j$$

$$CC_j = \frac{1}{\Delta x_j}\left(\frac{2\varphi_j(D_{sj}+D_{Bj})\varphi_{j+1}(D_{sj+1}+D_{Bj+1})}{\Delta x_j\varphi_{j+1}(D_{sj+1}+D_{Bj+1})+\Delta x_{j+1}\varphi_j(D_{sj}+D_{Bj})}\right)$$

$$DD_j = -\varphi_j\alpha_j C_0 - R_j. \tag{6}$$

Boundary conditions are imposed through two additional and infinitely small control volumes located at the top and the bottom of the calculation domain ($j = 0$ and $j = N + 1$) by giving the coefficients for these control volumes (BB_0, CC_0, DD_0, AA_{N+1}, BB_{N+1}, and DD_{N+1}) the appropriate values. Two types of boundary conditions are relevant: (1) the concentration at the boundary is known, and (2) the flux over the boundary is known. A known concentration is then assigned at the top of the calculation domain by the following values

$$BB_0 = 1 \qquad CC_0 = 0 \qquad DD_0 = \text{known concentration.} \tag{7}$$

A known concentration at the bottom of the calculation domain is assigned in the same way through AA_{N+1}, BB_{N+1}, and DD_{N+1}.

The second type of boundary conditions (a known flux) at the top of the calculation domain is introduced by letting j equal 1 in Eq. 4, and using that Δx_0 equals zero, which gives

$$\text{known flux} = -\frac{\varphi_1(D_{s1}+D_{B1})}{\frac{1}{2}\Delta x_1}(C_1 - C_0). \tag{8}$$

This equation, or condition, is imposed by giving the following values to BB_0, CC_0, and DD_0:

$$BB_0 = \frac{\varphi_1(D_{s1}+D_{B1})}{\frac{1}{2}\Delta x_1} \qquad CC_0 = -\frac{\varphi_1(D_{s1}+D_{B1})}{\frac{1}{2}\Delta x_1}$$

$$DD_0 = \text{known flux.} \tag{9}$$

A known flux at the bottom of the calculation domain is assigned in the same way through AA_{N+1}, BB_{N+1} and DD_{N+1}.

For known (or guessed) values of R_j and a set of known boundary conditions, C_j can be found by solving the tridiagonal system of linear equations (Eq. 5) using standard techniques, such as the Thomas algorithm (Patankar 1980). In most situations, this approach would lead to excessive calculation time because the tridiagonal system of equations is solved numerous times in this procedure. A much faster approach is possible. As Eq. 6 shows, AA_j, BB_j, and CC_j are functions of φ_j, α_j, D_{sj}, and D_{Bj}, and DD_j is a function of φ_j, α_j, C_{0j}, and R_j. Because all solutions of Eq. 5 are based on the same values of φ_j, α_j, D_{sj}, and D_{Bj}, the coefficients AA_j, BB_j, and CC_j will be constants during the multiple solutions, and DD_j will have different values because R_j varies. As Eqs. 7 and 9 show, this characteristic also holds for the equations containing the boundary conditions, even if the numeric value of the boundary conditions changes, as long as the type of boundary condition (a known flux or a known concentration) is the same. Thus, the problem to be solved can be characterized as a set of $N + 2$ linear equations with multiple right sides. This characteristic can be used to reduce the computational effort significantly by inverting (or decomposing) the matrix only once, after which each of the multiple solutions can be found with very little computational effort. In our implementation, we have used a rewritten version of the Thomas algorithm, which we have separated into two algorithms: one decomposing the matrix, and one using the decomposed matrix to produce multiple solutions. The details of rewriting the Thomas algorithm are not described here because similar pairs of algorithms can be found in commercial software libraries such as the IMSL Libraries or Numerical Recipes (Press et al. 1992).

To evaluate the quality of the different fits to the measured concentration profile, the following sum of squared deviations (or errors) is used:

$$\text{SSE} = \sum_{i=1}^{M} (Cm_i - \tilde{C}_i)^2, \tag{10}$$

where M is the number of measured concentrations, Cm_i is the measured concentration, and $\tilde{C}_i$ is the corresponding concentration interpolated from the calculated concentrations to the same depth as Cm_i.

To calculate a production profile, we must assume a unique functional dependence of the production rate with depth. In the current implementation, we have chosen to focus on piecewise-constant functions, each with a uniform production rate in each volume of sediment (referred to as zones below), as illustrated in Fig. 1. Such functions have been used for this purpose in several previous studies (Christensen et al. 1989; Rasmussen and Jørgensen 1992; Glud et al. 1994).

For simplicity, assume first a production profile where the number of zones, as well as their extent, is known. The independent variables that uniquely describe the profile are then limited to the production rates within each zone. Our goal is to find the particular combination of production rates that minimizes the deviation between the calculated and the measured concentration profile (Eq. 10). Minimization of such a function is a well-known problem, and many algorithms are available for this purpose (*see* for example the IMSL Libraries or Numerical Recipes; Press et al. 1992). We have used our own algorithm based on the Downhill Simplex Method (Nelder and Mead 1965).

Using piecewise-constant functions as production profiles requires that special precautions be taken. First, two adjacent zones with the same production rate can be regarded as one zone, which means that exactly the same production profile

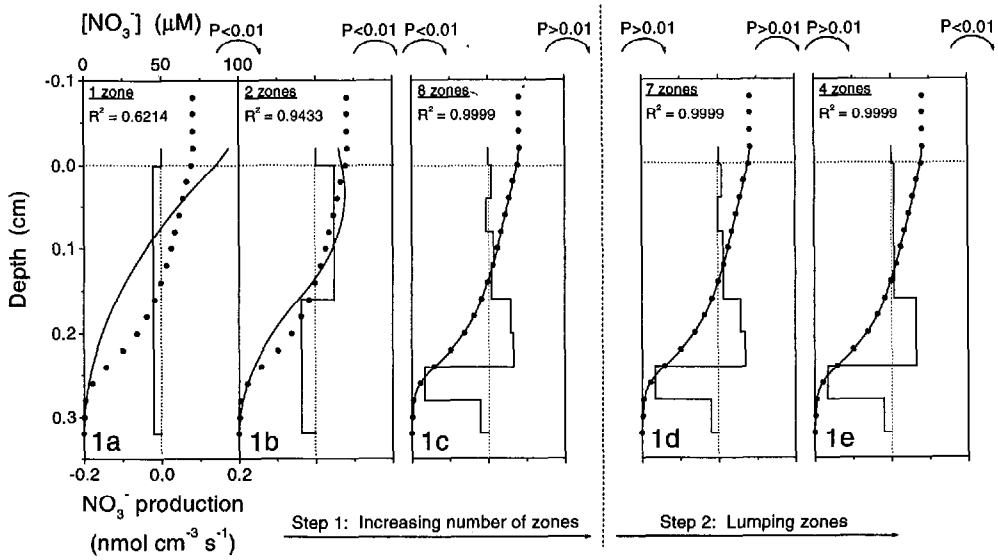

Fig. 1. The two steps in the procedure where measured data points (circles) are given as input, and the best-fitting concentration profiles (lines) and the production rates in the piecewise-constant production profiles (lines) are calculated. In the first step (a–c), the lowest number of equally spaced zones that provides a good explanation of the measured concentration profile is determined. In the second step (d, e), as many adjacent zones as possible are combined without reducing the quality of the fit obtained in the first step.

can be described in more than one way. With such lack of uniqueness, the risk of failure of the minimization process is high, and this problem exists as long as the number of zones (or their extent) is a variable in the minimization process. Second, data points that are slightly out of the range with the rest of the measurements should be included in the calculations, but they should not be allowed to define narrow zones of unusual production rates. Somehow a minimum extent to the zones must be included in the calculations.

A two-step procedure effectively avoids these problems. The first step of the procedure is to find the lowest number of equally spaced zones and the corresponding production rates that provide a good explanation for our measured concentration profile. The second step is to determine if some adjacent zones can be combined without reducing the quality of the fit obtained in the first step.

In the first step, as illustrated in Fig. 1a–c, an initial set of production profiles is constructed by subdividing the sediment column into increasing numbers of equally spaced zones, so that the first profile contains one zone with an unknown production rate, the second profile contains two zones, each with unknown production rates, and so on. These production rates are now determined independently by carrying out the minimization process for each profile. The result is a set of best fits to the measured concentration profile (*see* Fig. 1), each with a related minimum value of SSE (Eq. 10).

All fits are now compared in a series of statistical *F*-tests, as described by Kleinbaum and Kupper (1978). To make a choice between fits, the following null hypothesis is tested: given a number of zones (K), the addition of one or more zones does not significantly improve the prediction of the measured concentration profile. The hypothesis is tested by calculating the F value (Kleinbaum and Kupper 1978):

$$F = \frac{\dfrac{(\mathrm{SSE})_K - (\mathrm{SSE})_L}{L - K}}{\dfrac{(\mathrm{SSE})_L}{M - L}}, \tag{11}$$

where M is the number of measured concentrations and K and L are the numbers of zones in each of the two compared production profiles ($L > K$). From the F value, a probability (P value) is calculated from the F distribution, upon which the hypothesis is rejected or accepted.

The usual pattern is that adding an extra zone gives a better fit (smaller value of SSE). The opposite situation is also possible if the sediment studied contains an abrupt change in production rate at a certain depth and this abrupt change falls in the middle part of a zone when adding the extra zone. For that reason, a fit based on K zones must be compared with fits based on $K + 1$, $K + 2$, $K + 3$, ... zones. In this way, the first step of the procedure serves not only to determine the number of equally spaced zones adequate to describe the overall variation of the production profile but also to find the right separation into zones that covers any abrupt changes in production rates, if they exist. Table 1 shows an example of calculated values of SSE, R^2, and P (for the NO_3^- profile in Fig. 1) for 1–12 equally spaced zones. Increasing the number of zones from one to two and from two to three yields P values of 0.000, which means that the fits are getting significantly better with increasing number of zones. Increasing the number of zones further, from three to four, from three to five, and from three to six, results in P

Table 1. Sum of squared deviations (SEE), R^2 for the best obtainable fits with different numbers of equally spaced zones, and P values for testing the null hypothesis: the addition of one or more zones does not significantly improve the prediction of the measured concentration profile.

			Zones										
Zone	SSE	R^2	2	3	4	5	6	7	8	9	10	11	12
1	0.4248E+04	0.6214	0.000	0.000	0.000	0.000	0.000	0.000	0.000	0.000	0.000	0.000	0.000
2	0.6358E+03	0.9433		0.000	0.000	0.000	0.000	0.000	0.000	0.000	0.000	0.000	0.000
3	0.3593E+02	0.9968			1.000	1.000	0.012	0.000	0.000	0.000	0.000	0.000	0.000
4	0.4464E+02	0.9960				0.327	0.001	0.000	0.000	0.000	0.000	0.000	0.000
5	0.4134E+02	0.9963					0.001	0.000	0.000	0.000	0.000	0.000	0.000
6	0.1499E+02	0.9987						0.000	0.000	0.000	0.000	0.000	0.000
7	0.2184E+01	0.9998							0.000	0.008	0.005	0.032	0.031
8	0.6030E+00	0.9999								1.000	0.350	0.925	0.574
9	0.7413E+00	0.9999									0.060	0.389	0.257
10	0.4638E+00	1.0000										1.000	0.621
11	0.5663E+00	0.9999											0.159
12	0.3956E+00	1.0000											

values of 1.000, 1.000, and 0.012, respectively. Clearly the fits at four and five zones are not better than the three-zone fit, and demanding a level of significance ≤ 0.010 for rejection of the null hypothesis, neither is the six-zone fit. However, comparing the seven-zone fit with the three-zone fit yields a P value of 0.000, which also is obtained when going from seven to eight zones. Increasing the number of zones above eight gives P values larger than 0.010 in all situations. This means that the fits obtained for 9, 10, 11, and 12 zones are not significantly better than the 8-zone fit, making the 8-zone production profile (Fig. 1c) a clear choice. The high R^2 value of 0.9999 for eight zones further indicates that this choice is appropriate.

Some of the adjacent zones are likely to have almost similar production rates, and the possibility of lumping these zones is evaluated in the second step (Fig. 1d–e). Starting from the number of equally spaced zones found in step one (i.e., eight zones), the two adjacent zones with the most similar production rates (zones 3 and 4 in Fig. 1c) are now combined to equal one zone, and the minimization process is repeated. The result is a new fit (Fig. 1d) with a minimum value of SSE. The two next adjacent zones are combined following the same principles, and a new minimization is done. This process of minimization, followed by a reduction of the number of zones by one, is repeated until a production profile of only one zone is reached. As before, this new set of best fits is compared through F-tests as shown in Table 2. Decreasing the number of zones from eight to seven yields P values of 0.655, which means that the eight-zone fit is clearly not significantly better than the seven-zone fit. At a significance level of 0.010, the reduction from four to three zones is the first situation where the extra zone results in a significantly better fit, and the four-zone production profile (Fig. 1e) is chosen as the final result. Note that the R^2 values stay constant when reducing the number of zones from eight to four. The interpretation of this NO_3^- profile is discussed below.

All solutions of Eq. 1 are based on specified boundary conditions, one at the top and one at the bottom of the calculation domain. The fact that each solution is based on known values of R_j gives two additional options when specifying the boundary conditions. A typical example is the NO_3^- profile in Fig. 1, where the concentration, as well as the flux, at a certain depth is known to be zero. One obvious boundary condition is to specify a known concentration of zero at this depth. Because the flux also equals zero here, the flux at the top of the calculation domain can be calculated as the depth integration of R_j and used as the top boundary condition.

Table 2. Equivalent to Table 1, but for the second step of the procedure where adjacent zones are combined.

			Zones						
Zone	SSE	R^2	7	6	5	4	3	2	1
8	0.6030E+00	0.9999	0.655						
7	0.6158E+00	0.9999		0.424					
6	0.6545E+00	0.9999			0.026				
5	0.1005E+01	0.9999				0.728			
4	0.1015E+01	0.9999					0.000		
3	0.6966E+02	0.9938						0.513	
2	0.7175E+02	0.9936							0.000
1	0.4248E+04	0.6214							

Results and discussion

Test against analytical solutions—Three forms of solute transport are represented in Eq. 1: molecular diffusion, bioturbation, and irrigation. Without neglecting any of these, an analytical solution is possible if it is assumed that φ, D_s, D_B, and α are constant with depth. Although this is a limiting assumption from a practical perspective, it provides an excellent means by which to test the new procedure, because the only deviation between the analytical and the correct numerical solution is due to rounding errors, which should be very small. The following analytical solution can be found in the large selection of such solutions for diagenetic problems by Boudreau (1997):

$$C = A \exp\left(-\sqrt{\frac{\alpha}{D_s + D_B}}x\right) + B \exp\left(\sqrt{\frac{\alpha}{D_s + D_B}}x\right) + \frac{\alpha C_0 + \frac{R}{\varphi}}{\alpha}, \quad (12)$$

where A and B are arbitrary constants. This solution was used to calculate a hypothetical dissolved O_2 profile assuming different but constant consumption rates over the depth interval of 0–0.75 cm and 0.75–1.0 cm. The resulting two-step solution is extended through a diffusive boundary layer (−0.05–0 cm), where the analytical solution is given by a straight line. Labeling these three depth intervals 1, 2, and 3 starting from the top, the complete solution contains six constants: A_1 and B_1 for the diffusive boundary ($C = A_1 + B_1 x$), and in Eq. 12, A_2 and B_2 for the upper depth interval in the sediment and A_3 and B_3 for the lower depth interval.

The three solutions are connected through the following boundary conditions:

$$\begin{aligned} x = 1: &\quad C_3 = 0 \quad \text{and} \quad \frac{dC_3}{dx} = 0 \\ x = 0.75: &\quad C_2 = C_3 \quad \text{and} \quad \frac{dC_2}{dx} = \frac{dC_3}{dx} \\ x = 0: &\quad C_1 = C_2 \quad \text{and} \quad D\frac{dC_1}{dx} = \varphi(D_s + D_B)\frac{dC_2}{dx}, \end{aligned} \quad (13)$$

where D is the diffusivity of O_2 in free water. The bottom water concentration C_0 is defined as the concentration right above the diffusive boundary layer ($C_0 = A_1 - 0.05B_1$). Assuming O_2 consumption rates of 0.004 and 0.012 nmol cm^{-3} s^{-1} for the 0–0.75-cm and 0.75–1.0-cm intervals, respectively, and values of $\varphi = 0.75$, $D = 1.6 \times 10^{-5}$ cm^2 s^{-1}, $D_s = 0.9 \times 10^{-5}$ cm^2 s^{-1}, $D_B = 0.3 \times 10^{-5}$ cm^2 s^{-1}, and $\alpha = 5 \times 10^{-6}$ s^{-1}, the six constants obtain values of $A_1 = 355.167$, $B_1 = -320.195$, $A_2 = 966.257$, $B_2 = 84.4001$, $A_3 = 2697.19$, and $B_3 = 741.720$.

Based on a depth increment of 0.05 cm, 22 data points were calculated from this solution and used as input to the fitting procedure. The data points are shown in Fig. 2 with the results of the test, which were obtained with a separation

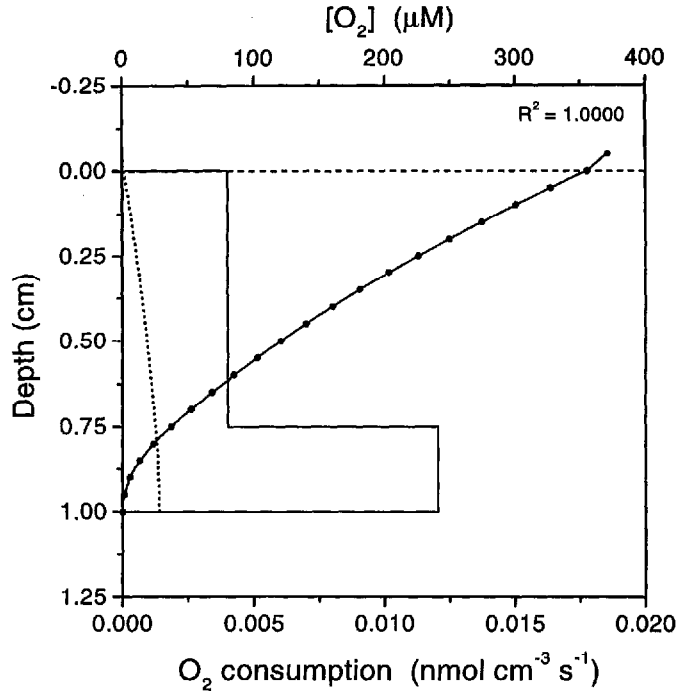

Fig. 2. Comparison against an analytical solution. Data points (circles) in the water column and in the sediment were calculated from the analytical solution. The sediment–water interface is located at depth 0 cm. The best fitting concentration profile (line), the influence of irrigation (dot), and the consumption profile were calculated by the procedure.

of the calculation domain (from −0.05 to 1.0 cm) into 400 control volumes. The calculated concentration profile fits the data points precisely, giving an R^2 value of 1.0000, and the calculated consumption rates (0.004001 and 0.01203 nmol cm^{-3} s^{-1}) are nearly equal to those assumed in the analytical solution. The diffusive flux (molecular diffusion and bioturbation) across the sediment–water interface was calculated to be 0.00512 nmol cm^{-2} s^{-1} and the depth-integrated effect of irrigation yields 0.00088 nmol cm^{-2} s^{-1}. The sum of these two values matches exactly the depth-integrated O_2 consumption of 0.00600 nmol cm^{-2} s^{-1} assumed in the analytical solution. In the first step of the procedure where the number of equally spaced zones was increased from one to six, the following minimum values of SSE (Eq. 10) were calculated: 670, 130, 13, 0.027, 1.4, and 1.2. The large decrease (a factor of 480) going from three to four zones followed by a significant increase (a factor of 50) going from four to five zones was calculated because the jump in consumption rate at depth 0.75 cm was exactly matched by one of the borders between the zones at the four-zone consumption profile. Similar results were found for the second step of the procedure when lumping the zones.

As an additional test, the response of the procedure to an abrupt change in consumption rate at a depth that is not matched exactly by one of the borders between the zones was examined. The jump in O_2 consumption was moved from 0.75 to 0.62 cm depth in the analytical solution, and

all other assumptions were left unchanged. From these calculations (starting the lumping from five equally spaced zones), the jump in O_2 consumption was predicted to be at a depth of 0.60 cm, and the two consumption rates were estimated to be 0.003885 and 0.01159 nmol cm^{-3} s^{-1}, which is within 3% of the rates assumed in the analytical solution. The procedure yields 0.00697 nmol cm^{-2} s^{-1} for the depth-integrated O_2 consumption, which matches the value of 0.00704 nmol cm^{-2} s^{-1} used in the analytical solution to within 1%.

Examples based on measured data—The procedure has been employed successfully with a variety of different types of measured data as input. Some illustrative examples from two field sites, one marine and one freshwater, are presented here with a discussion of the biogeochemical processes involved. All calculations were done with a separation of the calculation domains into 400 control volumes and at a level of significance of 0.01.

Pore water concentration profiles of O_2, NH_4^+, and ΣCO_2 were measured in sediment cores collected by scuba divers at 4 m depth in Skive Fjord, Denmark. Twenty sediment cores (5.3 cm diameter) were collected for measurements of O_2 fluxes across the sediment–water interface, porosity, and the concentration profiles. The sediment cores were immediately brought to the laboratory, and 10 sediment cores were sectioned in 3–10-mm slides for measurement of NH_4^+ and ΣCO_2 profiles (five replicates for each). From each sediment section, the pore water was extracted by squeezing through a glass-fiber filter under a pressure of 3–5 bar. A membrane (SDI rubber dam, Upplands Vaesby, Sweden) was placed above the sediment sample and the glass-fiber filter while squeezing. The pore water samples for NH_4^+ determination were frozen (−18°C) in 5-ml plastic vials for later analysis. Pore water samples for ΣCO_2 were placed in gas-tight vials (1.5-ml borosilicate glass vial with butyl rubber stoppers) and preserved with addition of $HgCl_2$. Concentrations of NH_4^+ and ΣCO_2 were measured on 100-μl samples using a small-volume flow injection technique described by Hall and Aller (1992). O_2 fluxes across the sediment–water interface were measured on five cores, as described by Rysgaard et al. (1995). After the flux measurement, all five cores were sieved through a 1.0-mm mesh screen to collect benthic animals. No animals were found. Microprofiles of O_2 were measured in the remaining five cores with a Clark-type O_2 electrode (Revsbech 1989*a*). During the measurements, the cores were submerged in a tank with water collected at the field site and kept at the in situ temperature. After the measurements, the cores were sliced into 3–10-mm sections, and sections from the same depth of each core were pooled for porosity determination by weight loss after drying. The porosity was 0.8 (vol/vol), and was constant at all depths.

The concentration profiles of O_2, NH_4^+, and ΣCO_2 were used as input for the numerical procedure. The diffusivities in water were 11.7 × 10^{-6} cm^2 s^{-1} for O_2 (Broecker and Peng 1974), 9.8 × 10^{-6} cm^2 s^{-1} for NH_4^+ (Li and Gregory 1974), and 9.4 × 10^{-6} cm^2 s^{-1} for ΣCO_2 (Li and Gregory 1974). The diffusivities corrected for tortuosity were calculated as $D_s = D\varphi^2$, according to Ullman and Aller (1982). Irrigation and bioturbation were neglected ($\alpha = 0$ and $D_B =$ 0) because no animals were found when the sediment was sieved.

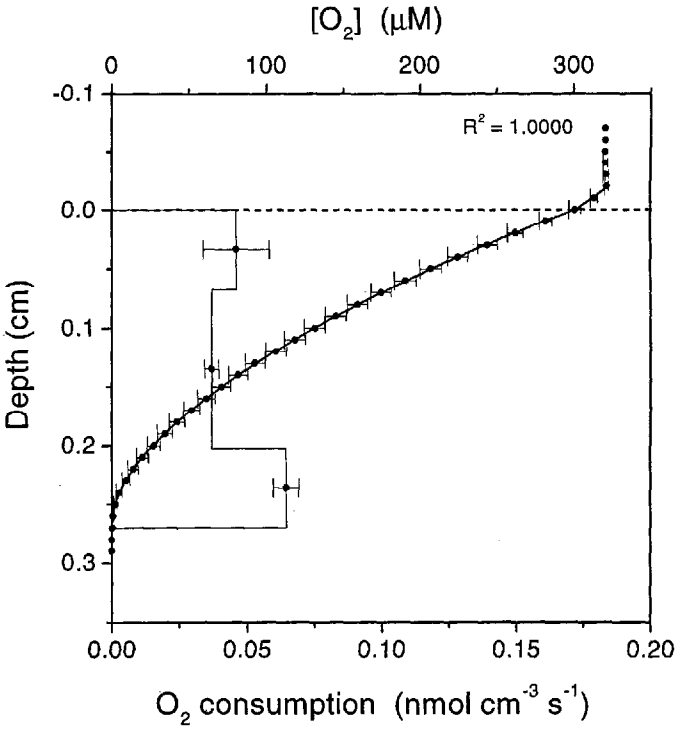

Fig. 3. Measured O_2 concentrations from a marine sediment, the calculated best-fitting concentration profile (line), and the connected consumption profile. Standard errors shown on the right side of the measured data points were calculated from the replicate concentration measurements, and standard errors on the left side were calculated from the fits to each single concentration profile. Standard errors shown on the consumption profile were calculated from rates related to the fits to each concentration profile.

The measured profile of O_2 is shown in Fig. 3, together with the calculated O_2 profile and the corresponding consumption profile. The calculated concentration profile fits the measured data points perfectly, both in the sediment and in the diffusive boundary layer (R^2 = 1.0000). The flux across the sediment–water interface was calculated to be 447 ± 29 μmol m^{-2} h^{-1}, where the standard error was calculated from fits to individual concentration profiles. This flux matches the flux measured in chambers of 484 ± 48 μmol m^{-2} h^{-1}. The standard errors shown in Fig. 3 on the right side of the measured data points were calculated from the replicate concentration measurements, and the standard errors on the left side were calculated from the fits to each single concentration profile. These two calculations of standard errors give the same result because each individually measured concentration profile is smooth and causes the individual fits to run through each data point. The standard errors shown on the consumption profile were calculated from rates related to the fits to each single concentration profile. The relatively large standard error on the upper zone reflects the natural variation in this sediment. The increased consumption rate at the bottom of the oxic layer is presumably due to oxidation of re-

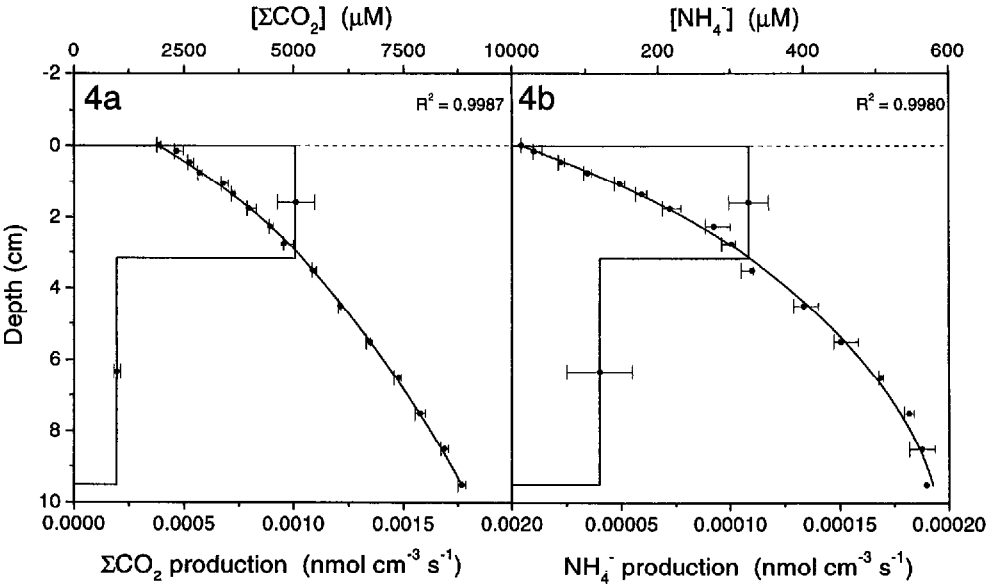

Fig. 4. Measured concentrations (circles) of ΣCO_2 (a) and NH_4^+ (b) from the marine sediment, the calculated best-fitting concentration profiles (lines), and the connected production profiles. Standard errors shown on the right side of the measured data points were calculated from the replicate measurements, and standard errors on the left side were calculated from the fits to each concentration profile. Standard errors shown on the production profiles were calculated from rates related to the fits to each concentration profile.

duced compounds (NH_4^+, Fe^{2+}, H_2S) diffusing up from below.

The results for the concentration profiles of ΣCO_2 and NH_4^+ are shown in Fig. 4. Although these two profiles have more variability than the O_2 profile presented previously, high R^2 values were calculated (0.9987 for ΣCO_2 and 0.9980 for NH_4^+). The production profiles consist of two distinct zones for both species, with the highest production rates in the upper portion of the sediment cores. These higher production rates reflect intense degradation of relatively recently deposited organic material. A comparison of the production rates with depth shows that approximately 50% of the total production of ΣCO_2 and NH_4^+ occurs in the upper 3.0 cm. The C:N ratio for the bioavailable organic material calculated from the depth-integrated production rates of ΣCO_2 and NH_4^+ is 7 for the analyzed sediment cores. This C:N ratio represents the C:N Redfield ratio of phytoplankton (Redfield 1934). The standard errors shown on the right side of the measured data points were calculated from the replicate measurements, and the standard errors on the left side were calculated from the fits to each single concentration profile. On average, the standard errors calculated from the fits are smaller than those calculated from the measured data because of the smoothing effect that is built into the fitting methodology. The standard errors shown on the production profiles were calculated from rates related to the fits to each concentration profile.

Microprofiles of O_2, NO_3^-, and NH_4^+ were also measured in a freshwater sediment from which benthic animals had been removed so that molecular diffusion was the only transport process. Sediment was collected in Lake Vilhelmsborg Sø, Denmark, and sieved through a 0.5-mm mesh screen to remove larger animals and coarse particles. The sediment was transferred to a glass chamber, and the water column above was continuously refreshed with aerated artificial freshwater (Lehman 1980) to which $NaNO_3$ (100 μM) had been added. The water column was mixed with a Teflon-coated magnetic stirbar. The glass chamber was kept in an open temperature-controlled (17.1°C) reservoir that was covered with dark plastic to prevent photosynthesis by benthic microalgae. Paired microprofiles of O_2–NO_3^- and O_2–NH_4^+ were measured simultaneously in the sediment after 15 days of incubation, at which time the experimental set-up should have reached steady state based on model simulations (Revsbech et al. 1986). Microprofiles of O_2 were measured with a Clark-type O_2 electrode (Revsbech 1989*b*), and NO_3^- microprofiles were measured with a shielded liquid-membrane ion selective microsensor (Jensen et al. 1993). Microprofiles of NH_4^+ were measured with a liquid-membrane ion-selective microsensor, based on the neutral carrier nonactin (de Beer and van den Heuvel 1988).

The diffusivity of O_2 in the sediment was determined using a high-resolution technique devised by Revsbech (1989*a*) and was found constant with depth at a value of 1.68×10^{-5} cm^2 s^{-1}. The free-solution diffusivities were 1.95×10^{-5} cm^2 s^{-1} for O_2 (Broecker and Peng 1974), 1.58×10^{-5} cm^2 s^{-1} for NO_3^- (Li and Gregory 1974), and 1.64×10^{-5} cm^2 s^{-1} for NH_4^+ (Li and Gregory 1974). The diffusivities of NO_3^- and NH_4^+ in the sediment were calculated to be 1.36×10^{-5} and 1.41×10^{-5} cm^2 s^{-1}, assuming that the ratio between the diffusivity in sediment and that in water is the same for these species as for O_2. The porosity was calculated to be 0.93 as $\varphi = \sqrt{D_s/D}$, according to Ullman and Aller (1982).

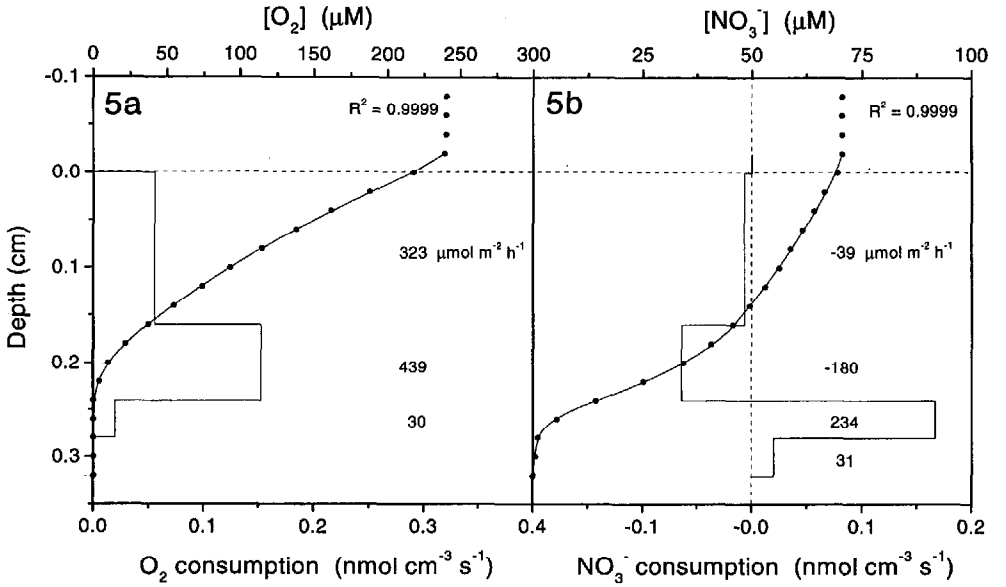

Fig. 5. Simultaneously measured concentrations (circles) of O_2 (a) and NO_3^- (b) from a freshwater sediment, the calculated best-fitting concentration profiles (lines), and the connected consumption profiles.

The measured pair of profiles of O_2–NO_3^- and O_2–NH_4^+ are shown in Figs. 5 and 6 with the results of the procedure, which gave a selection of fits with R^2 values of 0.9999, 0.9999, 0.9983, and 0.9997 for the profiles of O_2–NO_3^- and O_2–NH_4^+, respectively. Both O_2 consumption profiles (Figs. 5a, 6a) exhibit significant consumption at all depths, which was expected because the sediment was incubated in darkness to prevent photosynthesis. The calculated O_2 fluxes across the sediment–water interface for the two different O_2 profiles were alike (profile 5a: 792 µmol m^{-2} h^{-1}; profile 6a: 785 µmol m^{-2} h^{-1}), as were the consumption rates at the top of the profiles (profile 5a: 0.055 nmol cm^{-3} s^{-1}; profile 6a: 0.058 nmol cm^{-3} s^{-1}). Likewise, the maximum rates near the oxic–anoxic interface were similar (profile 5a: 0.152 nmol cm^{-3} s^{-1}; profile 6a: 0.151 nmol cm^{-3} s^{-1}), suggesting intensive oxidation of reduced compounds (e.g., NH_4^+) that were supplied by diffusion from below.

The results for the profiles of NO_3^- (Fig. 5b) and NH_4^+

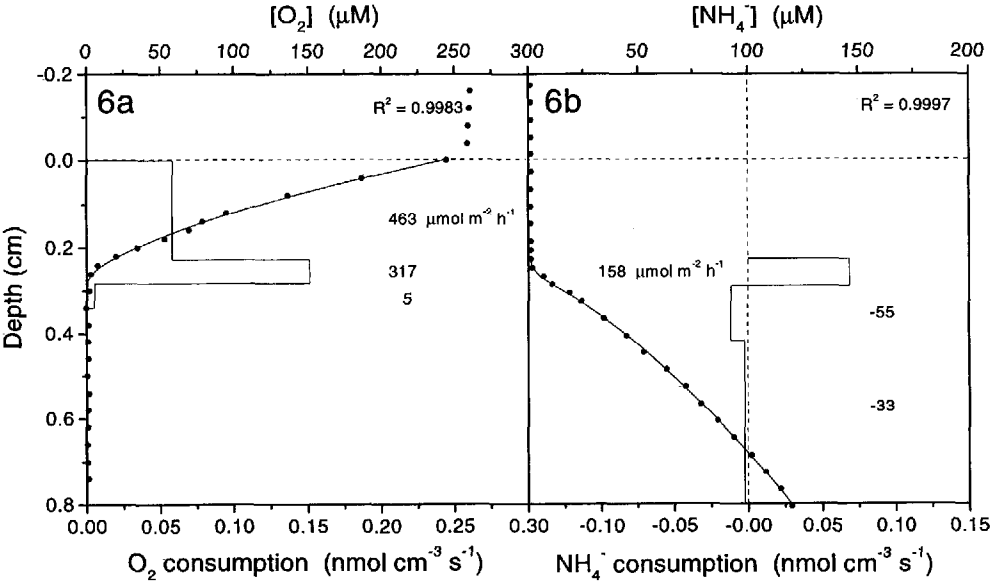

Fig. 6. Simultaneously measured concentrations (circles) of O_2 (a) and NH_4^+ (b) from the freshwater sediment, the calculated best-fitting concentration profiles (lines), and the connected consumption profiles.

(Fig. 6b) show zones of production as well as consumption. We attribute NO_3^- production to nitrification, NO_3^- consumption to denitrification, and NH_4^+ production to ammonification. Furthermore, NH_4^+ consumption is attributed to NH_4^+ oxidation (nitrification), because the depth-integrated NH_4^+ consumption at the bottom of the oxic layer almost matches NO_3^- production stoichiometrically over the same depth interval (158 vs. 180 μmol m^{-2} h^{-1}).

Two distinctive zones of nitrification were found (Fig. 5b), with a depth-integrated NO_3^- production of 219 μmol N m^{-2} h^{-1}. The maximum NO_3^- production was found just above the oxic–anoxic interface, and the depth-integrated production in this interval constituted about 82% of total nitrification. A similar inhomogenous depth distribution of nitrification, with maximum production near the anoxic–oxic interface, was also found by Jensen et al. (1994). As Fig. 6 indicates, the uneven depth distribution of nitrification was the consequence of NH_4^+ consumption just above the oxic–anoxic interface. The NH_4^+ that diffused into the oxic layer from the anoxic sediment below was consumed in the narrow lower oxic nitrification interval. Nitrification in the upper sediment was exclusively supported by NH_4^+ produced by aerobic degradation of organic-bound N. Nitrification in this depth interval was limited by NH_4^+, as indicated by the absence of NH_4^+ in the pore water. Denitrification took place in the sediment where O_2 concentrations were below 1 μM, which is consistent with denitrification as an anaerobic process. Because net NO_3^- production balanced NH_4^+ consumption in the lower nitrification interval, oxic denitrification at this depth was considered insignificant.

The examples presented and the discussion of the findings show that valuable information can be obtained by using modeling techniques for the interpretation of measured concentration profiles. The numerical procedure is an effective tool in studies of biogeochemical processes in sediments, and the procedure works well on profiles that differ in terms of shape, smoothness, number of data points, and scale.

Availability

The executable code of our procedure, PROFILE version 1.0, is available by e-mailing the corresponding author (pb8n@virginia.edu). The program runs on an IBM-compatible personal computer. For optimal performance, please specify the generation of the computer processor (486, Pentium, etc.).

References

ALLER, C. A. 1980. Quantifying solute distributions in the bioturbated zone of marine sediments by defining an average microenvironment. Geochim. Cosmochim. Acta **44:** 1955–1965.

———. 1983. The importance of the diffusive permeability of animal burrow linings in determining marine sediment chemistry. J. Mar. Res. **41:** 299–322.

BLACKBURN, T. H., N. D. BLACKBURN, K. JENSEN, AND N. RISGAARD-PETERSEN. 1994. Simulation model of the coupling between nitrification and denitrification in a freshwater sediment. Appl. Environ. Microbiol. **60:** 3089–3095.

BOUDREAU, B. P. 1984. On the equivalence of nonlocal and radial-diffusion models for porewater irrigation. J. Mar. Res. **42:** 731–735.

———. 1997. Diagenetic models and their implementation. Springer-Verlag.

BRANDL, H., AND K. W. HANSELMANN. 1991. Evaluation and application of dialysis porewater samplers for microbiological studies at sediment–water interfaces. Aquat. Sci. **53:** 55–73.

BROECKER, W. S., AND T.-H. PENG. 1974. Gas exchange rates between air and sea. Tellus **26:** 21–35.

CHRISTENSEN, P. B., L. P. NIELSEN, N. P. REVSBECH, AND J. SØRENSEN. 1989. Microzonation of denitrification activity in stream sediments as studied with a combined oxygen and nitrous oxide microsensor. Appl. Environ. Microbiol. **55:** 1234–1241.

DALSGAARD, T., AND N. P. REVSBECH. 1992. Regulating factors of denitrification in trickling filter biofilms as measured with oxygen–nitrous oxide microsensor. FEMS Microbiol. Ecol. **101:** 151–164.

DE BEER, D., AND J. C. VAN DEN HEUVEL. 1988. Response of ammonium-selective microelectrodes based on the neutral carrier nonactin. Talanta **35:** 728–730.

EMERSON, S. 1976. Early diagenesis in anaerobic lake sediments: Chemical equilibria in interstitial waters. Geochim. Cosmochim. Acta **40:** 925–934.

GLUD, R. N., J. K. GUNDERSEN, B. B. JØRGENSEN, N. P. REVSBECH, AND H. D. SCHULZ. 1994. Diffusive and total oxygen uptake of deep-sea sediment in the eastern South Atlantic Ocean: in situ and laboratory measurements. Deep-Sea Res. **41:** 1767–1788.

HALL, P. O. J., AND R. C. ALLER. 1992. Rapid, small-volume, flow injection analysis for ΣCO_2 and NH_4^+ in marine and freshwaters. Limnol. Oceanogr. **37:** 1113–1119.

HAVERKAMP, R., AND M. VAUCLIN. 1979. A note on estimating finite difference interblock hydraulic conductivity values for transient unsaturated flow problems. Water Resour. Res. **15:** 181–187.

HESSLEIN, R. H. 1976. An in situ sampler for close interval pore water studies. Limnol. Oceanogr. **21:** 912–914.

JENSEN, K., N. P. REVSBECH, AND L. P. NIELSEN. 1993. Microscale distribution of nitrification activity in sediment determined with a shielded microsensor for nitrate. Appl. Environ. Microbiol. **59:** 3287–3296.

———, N. P. SLOTH, N. RISGAARD-PETERSEN, S. RYSGAARD, AND N. P. REVSBECH. 1994. Estimation of nitrification and denitrification from microprofiles of oxygen and nitrate in model sediment systems. Appl. Environ. Microbiol. **60:** 2094–2100.

KLEINBAUM, D. G., AND L. L. KUPPER. 1978. Applied regression analysis and other multivariable methods. Duxbury.

KROM, M. D., P. DAVISON, H. ZHANG, AND W. DAVISON. 1994. High-resolution pore-water sampling with a gel sampler. Limnol. Oceanogr. **39:** 1967–1972.

KUIVILA, K. M., J. W. MURRAY, AND A. H. DEVOL. 1989. Methane production, sulfate reduction and competition for substrates in sediments of Lake Washington. Geochim. Cosmochim. Acta **53:** 409–416.

LEHMAN, J. T. 1980. Release and cycling of nutrients between planctonic algae and herbivores. Limnol. Oceanogr. **25:** 620–632.

LI, Y.-H., AND S. GREGORY. 1974. Diffusion of ions in sea water and in deep-sea sediments. Geochim. Cosmochim. Acta **38:** 703–714.

NELDER, J. A., AND R. MEAD. 1965. A simplex method for function minimization. Comput. J. **7:** 308–313.

NIELSEN, L. P., P. B. CHRISTENSEN, N. P. REVSBECH, AND J. SØRENSEN. 1990. Denitrification and oxygen respiration in bio-

films studied with a microsensor for nitrous oxide and oxygen. Microb. Ecol. **19:** 63–72.

PATANKAR, S. V. 1980. Numerical heat transfer and fluid flow. McGraw-Hill.

PELEGRI, S. P., L. P. NIELSEN, AND T. H. BLACKBURN. 1994. Denitrification in estuarine sediment stimulated by the irrigation activity of the amphipod *Corophium volutator*. Mar. Ecol. Prog. Ser. **105:** 285–290.

PRESS, W. H., S. A. TEUKOLSKY, W. T. VETTERLING, AND B. P. FLANNERY. 1992. Numerical recipes in FORTRAN. Cambridge Univ. Press.

RASMUSSEN, H., AND B. B. JØRGENSEN. 1992. Microelectrode studies of seasonal oxygen uptake in a coastal sediment: Role of molecular diffusion. Mar. Ecol. Prog. Ser. **81:** 289–303.

REDFIELD, A. C. 1934. On the proportion of organic derivatives in sea water and their relation to the composition of plankton, p. 176–192. *In* James Johnston memorial volume. Univ. Press of Liverpool.

REEBURGH, W. S. 1967. An improved interstitial water sampler. Limnol. Oceanogr. **12:** 163–165.

REVSBECH, N. P. 1989*a*. Diffusion characteristics of microbial communities determined by use of oxygen microsensors. J. Microbiol. Methods **9:** 111–122.

———. 1989*b*. An oxygen microelectrode with a guard cathode. Limnol. Oceanogr. **34:** 474–478.

———, B. B. JØRGENSEN, T. H. BLACKBURN. 1980. Oxygen in the sea bottom measured with a microelectrode. Science **207:** 1355–1356.

———, B. MADSEN, AND B. B. JØRGENSEN. 1986. Oxygen production and consumption in sediments determined at high spatial resolution by computer simulation of oxygen microelectrode data. Limnol. Oceanogr. **31:** 293–304.

RYSGAARD, S., AND P. BERG. 1996. Mineralization in a northeastern Greenland sediment: Mathematical modelling, measured sediment pore water profiles and actual activities. Aquat. Microb. Ecol. **11:** 297–305.

———, P. B. CHRISTENSEN, AND L. P. NIELSEN. 1995. Seasonal variation in nitrification and denitrification in estuarine sediment colonized by benthic microalgae and bioturbating infauna. Mar. Ecol. Prog. Ser. **126:** 111–121.

SAYLES, F. L., P. C. MANGELSDORF, JR., T. R. S. WILSON, AND D. N. HUME. 1976. A sampler for the in situ collection of marine sedimentary pore waters. Deep-Sea Res. 23: 259–264.

THAMDRUP, B., K. FINSTER, AND H. FOSSING. 1994*a*. Thiosulfate and sulfite distributions in porewater of marine sediments related to manganese, iron, and sulfur geochemistry. Geochim. Cosmochim. Acta **58:** 67–73.

———, R. N. GLUD, AND J. W. HANSEN. 1994*b*. Manganese oxidation and in situ manganese fluxes from a coastal sediment. Geochim. Cosmochim. Acta **58:** 2563–2570.

ULLMAN, W. J., AND R. C. ALLER. 1982. Diffusion coefficients in nearshore marine sediments. Limnol. Oceanogr. **27:** 552–556.

WANG, Y., AND P. VAN CAPPELLEN. 1996. A multicomponent reactive transport model of early diagenesis: Application to redox cycling in coastal marine sediments. Geochim. Cosmochim. Acta **60:** 2993–3014.

Received: 2 January 1997
Accepted: 27 May 1998
Amended: 8 June 1998